



Cite this: *Catal. Sci. Technol.*, 2021, 11, 671

A new dynamic N_2O reduction system based on Rh/ceria-zirconia: from mechanistic insight towards a practical application†

Yixiao Wang,^{*ab} Jorrit Postuma de Boer^a and Michiel Makkee  ^{*a}

Simultaneous reduction of N_2O in the presence of co-existing oxidants, especially NO, from industrial plants, is a challenging task. This study explores the applications of a hydrocarbon reduced Rh/Zr stabilized La doped ceria (Rh/CLZ) catalyst in N_2O abatement from oxidant rich industrial exhaust streams e.g. NO, CO_2 , and O_2 . The reaction mechanism was studied by the temporal analysis of products. The obtained results revealed that hydrocarbon pretreatment led to the creation of ceria oxygen vacancies and the formation of carbon deposits on the Rh/CLZ catalyst surface. These ceria oxygen vacancies are the active sites for the selective reduction of N_2O into N_2 , while the dissociated O atoms from N_2O fill the ceria oxygen vacancies. The oxidation of the deposited carbon *via* the lattice ceria oxygen generates new ceria oxygen vacancies, thereby extending the catalytic cycle. The reduction of N_2O over C_3H_6 reduced Rh/CLZ is a process combining oxygen vacancy healing and deposited carbon oxidation. The results obtained from fixed-bed reactor experiments demonstrated that the hydrocarbon reduced Rh/CLZ catalyst provided a unique and extraordinary N_2O abatement performance in the presence of co-existing competing oxidants (reactivity order: $\text{N}_2\text{O} \sim \text{NO} > \text{O}_2 > \text{CO}_2 \sim \text{H}_2\text{O}$).

Received 16th October 2020,
Accepted 2nd November 2020

DOI: 10.1039/d0cy02035d

rsc.li/catalysis

1. Introduction

N_2O is a harmful gas to our environment, as it contributes to global warming and the depletion of the protective ozone layer. Human activities, *e.g.*, agriculture, fossil fuel combustion, and industrial processes, contribute 4.7–7 million tons of N_2O annually, which is about 30–40% of the total N_2O emission including natural sources.¹

The catalytic reduction of N_2O into N_2 has been studied over a wide variety of catalysts, including noble-metal-supported catalysts, metal oxides, and zeolite-based catalysts.² Several CeO_2 -based transition-metal catalysts (M/CeO_2 , $\text{M} = \text{Co, Cu, Fe, Zr, and Ni}$) have been applied in N_2O reduction studies. Their T_{50} temperature for the N_2O reduction varied between 300–660 °C.^{3–6} The impact of H_2O , CO , CO_2 , O_2 , NO , and NO_2 on N_2O reduction is particularly important, since these substances are usually present in excess in N_2O -containing gas streams. In particular, the simultaneous conversion of N_2O and NO in the presence of O_2 is a challenging task during N_2O abatement in nitric acid plants.

A lot of research efforts have been directed towards the development of low temperature de N_2O catalysts, which target N_2O abatement arising from medical operating rooms, nitric acid plants, and automotive transport.^{7,8} In all these cases, apart from the activity at low temperatures, the tolerance to various substances present in the exhaust gases (*e.g.*, NO_x , O_2 , H_2O , *etc.*) should be additionally addressed and subsequently enhanced. Few studies have addressed the simultaneous abatement of NO_x and N_2O . The current N_2O abatement in industry is usually *via* a dual-bed catalytic system, in which NO_x is firstly converted into N_2 by either $\text{NH}_3\text{-SCR}$ or HC-SCR , while subsequently N_2O is catalytically decomposed into N_2 and O_2 .^{9–11} Sufficient performance has rarely been achieved in a single catalyst bed.^{12–14} In particular, the N_2O abatement activity is strongly inhibited by the presence of NO .¹²

The Di-Air system, developed by Toyota Company, showed great promise in NO_x abatement with regard to the current and future NO_x emission standards under real driving automotive conditions (dynamic operations, high exhaust temperature, and high gas hourly space velocities ($\text{GHSV} > 120\,000 \text{ L L}^{-1} \text{ h}^{-1}$)).¹⁵ The comprehensive work by Wang and Makkee has addressed the working principle and application of this Di-Air system in NO reduction.^{16–21} Oxygen vacancies within the ceria lattice of a reduced ceria, Pt/ceria or Rh/ceria were found to be the selective catalytic sites for the NO reduction into only N_2 (100% selectivity).¹⁶ Even at low NO

^a Catalysis Engineering, Chemical Engineering Department, Faculty of Applied Sciences Delft University of Technology, Van der Maasweg 9, 2629 HZ Delft, The Netherlands. E-mail: m.makkee@tudelft.nl

^b Idaho National Laboratory, Idaho Falls, Idaho 83415, USA. E-mail: Yixiao.wang@inl.gov

† Electronic supplementary information (ESI) available. See DOI: [10.1039/d0cy02035d](https://doi.org/10.1039/d0cy02035d)



concentrations (ppm levels), NO could compete for oxygen vacancies with (100×) excess of O₂ and CO₂.²¹ These oxygen vacancies acted as a kind of “oxygen black hole” by catching all oxygen containing species until the holes (vacancies) were completely refilled (re-oxidized), while the captured N species would associate (recombine) into N₂. In the Di-Air system, the creation of reduced (noble metal) ceria was accomplished by pulsing diesel fuel at a high frequency upstream of the catalyst bed. The amount of diesel pulsed was such that the front of the catalyst bed was in a reduced state while the back of the catalyst bed was in an oxidized state. In other words, although diesel fuel is injected, the overall catalytic bed would be in a lean (oxidized) state. During these diesel pulses carbon deposits were formed, which were oxidized in time by the lattice oxygen from the ceria catalyst and not by gaseous oxidants present in the exhaust stream such as O₂ and NO_x (mainly NO₂).

To the best of our knowledge, no work has been published on the application of this “oxygen black hole” concept of the Di-Air system in a deN₂O application. In this study, we investigated the mechanism of the N₂O reduction over a reduced Rh/CLZ catalyst with a clean surface and with carbon deposits on that surface.

The temporal analysis of products (TAP, an ultra-high vacuum pulse and response technique) was applied to study the reaction mechanism of the N₂O reduction over a reduced Rh/CLZ catalyst, pre-treated with either H₂ or C₃H₆ as a stand-in for a diesel fuel. Moreover, the reactivity of N₂O *versus* other oxidants (O₂ and NO) towards oxygen vacancies of ceria-based catalysts would be crucial for the extension of the Di-Air technology to the deN₂O area, *i.e.*, the simultaneous NO_x and N₂O abatement in the presence of an excess of O₂. The competition between N₂O and NO in an excess of O₂ was further investigated under more industrially relevant conditions in a fixed-bed flow reactor.

2. Materials and methods

2.1. Materials preparation and characterization

Rh/CLZ, with a target loading of 0.5 wt%, was prepared *via* an incipient wetness impregnation method using a Zr stabilized La doped ceria (denoted as CLZ, a gift from Engelhard, now BASF). Rhodium(III) nitrate hydrate (Sigma Aldrich) was used and dissolved as the precursor in purified demi water. Subsequently, the samples were dried at 110 °C overnight and calcined at 550 °C for 5 h. CLZ and Rh/CLZ were characterized by ICP, XRD, TEM, XPS, Raman, and H₂-TPR. Details on the characterization and instruments can be found in our previous publications.^{16–21}

2.2. Catalytic testing

2.2.1. Temporal analysis of products (TAP). The pulse experiments (step-response) were performed in an in-house developed and constructed TAP reactor. The mode of the gas transport within the TAP catalyst is purely Knudsen diffusion. Upon interaction with the catalyst, the reactant and product

molecules can be converted into different products. The evolution of the reactant and product molecules was tracked (one mass at a time) in time with a high time resolution of 10 kHz using a Pfeiffer QMG 422 quadrupole mass spectrometer. The pulse size gradually decreased during an experiment since the reactant was pulsed from a closed and calibrated volume of the pulse-valve line. The pulse size of the reactant gas was determined for each pulse by fitting the pulse valve pressure using an exponential equation and compensation for the environmental temperature. All relevant MS signals were calibrated and quantified at room temperature by using an inert bed of 200 mg quartz beads (particle size 150–212 µm) fully filled in a stainless-steel SS 316 reactor. Detailed TAP quantification methods can be found elsewhere.¹⁶

In the TAP experiments at 450 °C 10 mg of as-prepared CLZ and Rh/CLZ (150–212 µm) were sandwiched between inert quartz bead beds. Prior to the catalyst reduction, the catalyst was firstly oxidized by pulsing 80 vol% O₂ in Ar overnight at 450 °C. The catalyst reduction was carried out by pulsing the reductant of either 80 vol% C₃H₆ (propene) in Ne or 66.7 vol% H₂ in Ar. The re-oxidation experiment was conducted at 450 °C by pulsing either 80 vol% CO₂ or 80 vol% O₂ in Ar, or 80 vol% ¹⁵N₂O in Kr, or co-pulsing 80 vol.% ¹⁴NO in He and 80 vol.% ¹⁵N₂O in Kr.

The number of consumed oxygen species from the catalyst during the C₃H₆ and H₂ multi-pulse experiments was calculated using eqn (1):

$$n_{O,\text{consumed}} = n_{H_2O,\text{out}} + n_{CO,\text{out}} + 2n_{CO_2,\text{out}} \quad (1)$$

and the number of carbon species deposited on the catalyst in the C₃H₆ multi-pulse experiments was calculated using eqn (2):

$$n_{C,\text{deposited}} = 3n_{C_3H_6,\text{in}} - 3n_{C_3H_6,\text{out}} - n_{CO,\text{out}} - n_{CO_2,\text{out}} \quad (2)$$

The number of oxygen atoms consumed during the C₃H₆ and H₂ multi-pulse experiments was equal to the number of oxygen vacancies created in the ceria lattice.

Similarly, the amount of oxygen accumulation, the carbon consumption, and the nitrogen balance during the ¹⁵N₂O, CO₂, and O₂ multi-pulse experiments were calculated using the following atomic balances:

$$n_{O,\text{accumulated}} = n_{N_2O,\text{in}} - n_{CO,\text{out}} - 2n_{CO_2,\text{out}} - n_{N_2O,\text{out}} - 2n_{NO_2,\text{out}} - n_{NO,\text{out}} \quad (3)$$

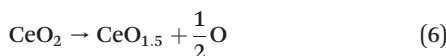
$$n_{C,\text{accumulated}} = -n_{C,\text{in}} - n_{CO,\text{out}} - n_{CO_2,\text{out}} \quad (4)$$

$$n_{N,\text{accumulated}} = 2n_{N_2O,\text{in}} - 2n_{N_2O,\text{out}} - 2n_{N_2O,\text{out}} - n_{NO,\text{out}} - n_{NO_2,\text{out}} \quad (5)$$

The hypothetical ceria layer concept was used to obtain insight into the reactivity of the actual surface as a function of the degree of reduction (surface oxidation state). Each O-Ce-O tri-layer on the (BET) surface was regarded as one hypothetical ceria layer. The total number of O atoms in each



hypothetical ceria layer can be calculated to be 1.04×10^{18} atoms per mg_{cat} . Assuming that Zr and La were Ce, a maximum of 25% of the total number of O ions in each crystal layer can be reduced, according to eqn (6)



The number of oxygen defects on one hypothetical reduced ceria layer was calculated to be 2.6×10^{17} oxygen atoms per mg_{cat} . More details about these calculations with regard to the hypothetical ceria layer can be found elsewhere.¹⁶

2.2.2. Reactivity measurement in a flow reactor. A flow reactor was used to study the N_2O reduction reactivity with and without O_2 and NO. The as-prepared catalyst (200 mg) with particle sizes between 150 and 215 μm was placed in a 6 mm inner-diameter quartz reactor tube. The reactor effluent was online analyzed by mass spectrometry (MS, Hiden Analytical, HPR-20 QIC) and infrared (IR) spectroscopy (Perkin-Elmer, Spectrum One). For the IR analysis a gas cell with KBr windows with a path length of ~ 5 cm was used. The spectra were measured in continuous mode using the Perkin-Elmer 'Time-Base' software between wavenumbers of 4000–700 cm^{-1} with a spectral resolution of 8 cm^{-1} and an acquisition rate of 8 scans per spectrum, resulting in a time interval of 23 s between each acquired spectrum. In all experiments, the catalyst was initially oxidized by O_2/He until the O_2 signal reached a stable level in MS. The reduction of the catalyst was performed by flowing 1.25% C_3H_6 in He for 2 h with a flow rate of 200 mL min^{-1} and subsequently flushing with He (200 mL min^{-1}) for 30 min at 450 °C. For the N_2O reduction experiments, feed composition of either 2000 ppm $\text{N}_2\text{O}/\text{He}$ or (2000 ppm $\text{N}_2\text{O} + 5\% \text{O}_2$)/He or (2000 ppm $\text{N}_2\text{O} + 2000$ ppm NO)/He was used at a space velocity of 67 000 $\text{L L}^{-1} \text{h}^{-1}$, at 450 °C.

3. Results and discussion

3.1. Structure, composition, and texture properties

Characterization details of the CLZ support and Rh/CLZ catalyst were reported in detail elsewhere.^{16–21} In brief, a 0.5 wt% Rh loading was confirmed by ICP-OES (0.0486 mmol $\text{g}_{\text{cat}}^{-1}$ Rh loading). A typical fluorite structure of CLZ was observed for both CLZ and Rh/CLZ samples by Raman as well as XRD. Rh metals or any rhodium oxides could not be observed by XRD, confirming a high Rh dispersion. Room temperature Raman results indicated that the Rh/CLZ samples had more oxygen vacancies as compared to CLZ.¹⁸ A 5 nm ceria crystal size was determined by the Scherrer equation (XRD) and was further confirmed by the analysis of the TEM micrographs. The particle size of Rh was around 2 nm as indicated in the TEM micrographs. The bulk composition of CLZ, with an atomic ratio of Ce, Zr, and La of 0.64:0.15:0.21, was determined by ICP. The BET surface area of bare (fresh and up to >2000 h time on stream) CLZ was $65 \text{ m}^2 \text{ g}^{-1}$. The BET surface areas of Rh/CLZ (fresh and spent) were similar to that of the bare CLZ support ($66 \pm 2 \text{ m}^2 \text{ g}^{-1}$).

3.2. Transient N_2O reduction

3.2.1. The role of oxygen vacancies and deposited carbon.

H_2 and C_3H_6 were applied as reductants to pretreat the Rh/CLZ catalyst samples at 450 °C in order to obtain a reduced Rh/CLZ sample and a reduced Rh/CLZ sample with deposited carbon on its surface, respectively. The H_2 pulses led only to H_2O formation (Fig. S4†)¹⁶ and the C_3H_6 pulses led to the formation of H_2O , CO_2 , CO , H_2 , and carbon deposits (Fig. S5†).¹⁸ By means of eqn (1) and (2), the total amount of oxygen vacancies and carbon deposits formed during the H_2 and C_3H_6 pulses could be obtained. A total amount of 2.0×10^{17} oxygen vacancies per mg_{cat} formed during the 1.3×10^4 pulses of H_2 , which corresponded to a reduction of 0.8 hypothetical ceria layers. During the 1.0×10^4 pulses of C_3H_6 , 5.3×10^{17} oxygen vacancies per mg_{cat} were formed and 2.6×10^{17} carbon atoms per mg_{cat} were deposited, which corresponded to a reduction of 2.2 hypothetical ceria layers. The pure CLZ support was barely active towards H_2 and C_3H_6 . The reduction of CLZ by H_2 at 450 °C led to 6×10^{16} oxygen vacancies per mg_{cat} , which corresponded to a reduction of 0.2–0.3 hypothetical ceria layers (see Fig. S2 in the ESI†). The presence of Rh promoted the reduction of CLZ at a lower temperature with a deeper degree of reduction.

Fig. 1A shows the reactant and product evolution during a $^{15}\text{N}_2\text{O}$ pulse experiment over H_2 reduced Rh/CLZ at 450 °C. A $^{15}\text{N}_2\text{O}$ conversion of 100% was observed, while $^{15}\text{N}_2$ was observed as the only N containing product from pulse numbers of 0 to 3400 (Fig. 1A, reduced state of Rh/CLZ). ^{15}NO was not observed during the whole experiment. There was no indication of any ^{15}N species accumulation on the catalyst (Fig. 1B), which suggested that N_2O was instantaneously reduced into N_2 with 100% selectivity. Oxygen atoms were observed to accumulate incrementally within the catalyst and 99% of the oxygen vacancies were refilled during the first 3400 $^{15}\text{N}_2\text{O}$ pulses. The results shown in Fig. 1 suggested that the N_2O reduction over the reduced Rh/CLZ catalyst was an oxygen vacancy refilling process, which was also evidenced by *in situ* Raman and XPS results from the study by Bueno-López *et al.*²² Gradually a $^{15}\text{N}_2\text{O}$ breakthrough was observed after pulse number 3400 (Fig. 1A), corresponding to a $^{15}\text{N}_2\text{O}$ conversion of roughly 95%. From pulse number 3400 onwards, the Rh/CLZ catalyst became completely oxidized and O_2 evolution was observed. From this point on the N_2O reduction proceeded *via* adsorbed O species recombination forming gas phase O_2 thereby regenerating two active sites, *e.g.*, reduced Rh metal sites and ceria oxygen vacancy sites. A slightly lower $^{15}\text{N}_2\text{O}$ conversion was observed when the catalyst was in a fully oxidized state (Fig. 1A), as compared to the reduced state. This was likely caused by a slower 'O' association into O_2 over the oxidized Rh/CLZ surface. The $\text{O}_{2(\text{g})}$ formation process consisted of a surface 'O' association step and an $\text{O}_{2(\text{g})}$ desorption step. In order to elucidate the slow $\text{O}_{2(\text{g})}$ formation step, O_2 was pulsed over an oxidized Rh/CLZ surface at the same temperature as the N_2O pulse experiment. As shown in Fig. S1,† a clear O_2 response was observed during the O_2 pulses, while no clear O_2 desorption curve was observed during



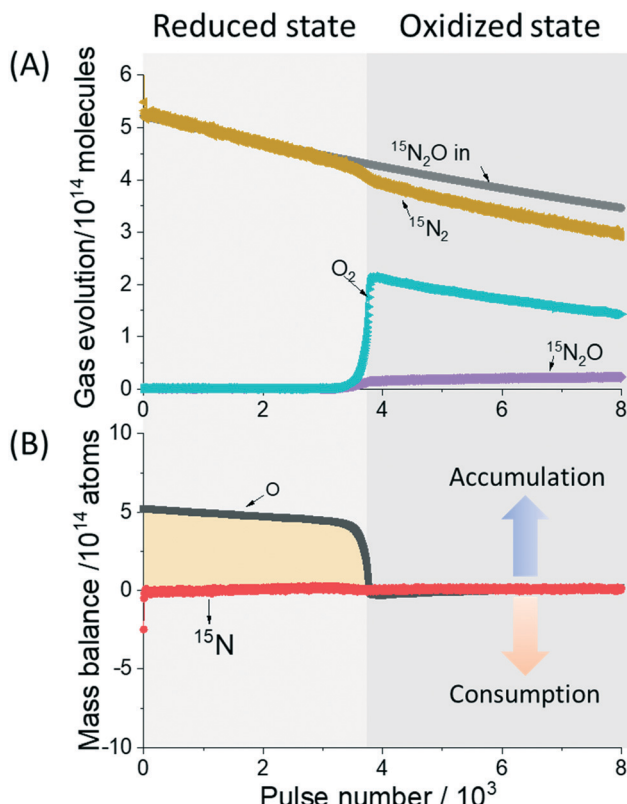


Fig. 1 A) Product and reactant evolution and B) O and N balance versus pulse number during the $^{15}\text{N}_2\text{O}$ multi-pulse experiment over H_2 reduced Rh/CLZ at $450\text{ }^\circ\text{C}$.

the N_2O pulses over an oxidized Rh/CLZ surface. Therefore, a slow 'O' association step was likely the cause of the slow O_2 desorption over the oxidized Rh/CLZ surface during N_2O reduction. A similar dynamic trend was observed with the H_2 pre-reduced CLZ bare support under the same reaction conditions (Fig. S2, ESI†) although the time until 100% $^{15}\text{N}_2\text{O}$ conversion was shorter due to the significantly lower reduction degree for the H_2 reduction of CLZ. In this case, a full conversion of $^{15}\text{N}_2\text{O}$ into $^{15}\text{N}_2$ was observed when the CLZ was in a reduced state. After that, the N_2 production decreased with a lower N_2O reduction activity (only 12% conversion of N_2O). The results obtained for the reduced CLZ (Fig. S2, ESI†) indicated that the N_2O reduction was an oxygen vacancy refilling process as well. From Fig. 1 and S2† it follows that the total amount of N_2O converted over the reduced catalysts was equal to the total amount of oxygen vacancies created during the H_2 reduction. Therefore, the role of Rh is to increase the CLZ support reduction degree by the H_2 reduction process. The presence of Rh did not noticeably alter the N_2O reduction rate, since 100% N_2O conversion was observed over reduced Rh/CLZ and CLZ. However, over oxidized CLZ the presence of Rh led to a significant improvement in the N_2O reduction activity, as the conversion of N_2O over oxidized Rh/CLZ was approximately 8 times that over oxidized CLZ. From *in situ* XPS results obtained for a Rh/ CeO_2 system by Parres-Escalapez *et al.*,²² it was known that the reduced rhodium sites could be re-oxidized afterwards by

either N_2O or ceria lattice oxygen. These vacant oxygen positions in ceria were subsequently oxidized by N_2O . The active sites for the N_2O chemisorption and reduction were not only located on rhodium, but were also present on the ceria. Additionally, Rh was a powerful promoter in enhancing the surface oxygen diffusion and lowering the oxygen activation barrier,^{23,24} and therefore, Rh could promote a faster surface oxygen association and desorption of gas-phase O_2 on the oxidized catalyst surfaces during the N_2O reduction. Rh could be a distinctive mechanistic feature for the promotion of the N_2O reduction process.²⁵

Transient N_2 formation during the $^{15}\text{N}_2\text{O}$ pulses was compared between the H_2 reduced Rh/CLZ and CLZ samples as shown in Fig. 2. In these experiments exclusively $^{15}\text{N}_2$ was observed as a reaction product. No observable N_2 flux difference was observed, which suggested that N_2O most likely reacted on the same reaction sites. These active sites were most likely the surface oxygen vacancies on the reduced CLZ support. The reduction of N_2O led to the oxidation of Ce^{3+} to Ce^{4+} , while N_2 was released. If two active sites should exist, *i.e.*, oxygen vacancies on the reduced CLZ support and Rh, then two distinguishable responses would have been expected^{26–28} rather than a single peak response that was observed in the current experiment. The hypothesis that only oxygen vacancy active sites were used on the reduced CLZ even in the presence of Rh explained the observed 100% $^{15}\text{N}_2\text{O}$ conversion over both reduced CLZ and Rh/CLZ. The results presented in Fig. 1, S2† and 2 all indicated that the oxygen vacancies on CLZ were the only active sites for the N_2O reduction. During the N_2O reduction, the O species refilled the CLZ lattice oxygen vacancies and N_2 desorbed to the gas phase. The role of Rh was the promotion of the deep CLZ reduction at lower temperatures, however this deep reduction had an insignificant impact on the N_2O reduction, when the catalyst was in a reduced state, *i.e.*, the presence of ceria oxygen vacancies. The presence of Rh started to promote the N_2O reduction only when the catalyst was in an oxidized state, *i.e.*, the absence of ceria oxygen vacancies.

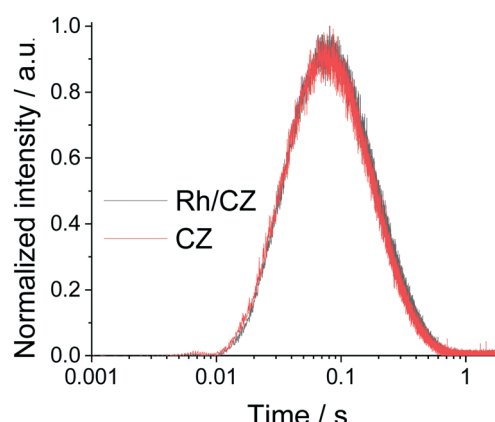


Fig. 2 Comparison of the height normalized intensity of $^{15}\text{N}_2$ between the H_2 reduced Rh/CLZ sample and reduced CLZ sample during the $^{15}\text{N}_2\text{O}$ pulses.



The investigation of the impact of deposited carbon on N_2O reduction is presented in Fig. 3. Fig. 3A shows the reactant and product evolution achieved over C_3H_6 reduced Rh/CLZ at 450 °C *versus* the incremental pulse number. Full $^{15}\text{N}_2\text{O}$ conversion was observed until pulse number 4500, while $^{15}\text{N}_2$ evolved as the dominant product. From pulse number 45 000 onward, a progressive, but small decline in the $^{15}\text{N}_2\text{O}$ conversion to 95% was observed. This decline was accompanied by the formation of O_2 , while hardly any CO and/or CO_2 was formed at this stage. No ^{15}NO was observed during the whole experiment.

A small amount of CO evolution was observed during the first 15 000 $^{15}\text{N}_2\text{O}$ pulses, during this time frame 80% of the ceria oxygen vacancies were refilled, while only 10% of the deposited carbon was consumed (Fig. 3B). This indicated that the carbonaceous residues, left on the surface after the C_3H_6 pre-reduction, did not directly participate in the reduction of $^{15}\text{N}_2\text{O}$ into $^{15}\text{N}_2$. The formation of $^{15}\text{N}_2$ indicated that $^{15}\text{N}_2\text{O}$ was dissociated on reduced CLZ sites, the O atom of $^{15}\text{N}_2\text{O}$ refilled the ceria oxygen vacancies and at the same time the remaining adsorbed $^{15}\text{N}_2$ species desorbed as $^{15}\text{N}_2$. A significant role of the direct reaction between $^{15}\text{N}_2\text{O}$ and deposited carbon could be ruled out since the formation of a $^{15}\text{N}_2$ molecule would yield one CO molecule, according to eqn (7).



The majority of deposited carbon consumption was found from pulse number 15 000 onward in the form of CO_2 . Oxygen accumulation dropped to zero starting from pulse number 20 000, at that point almost 100% of the oxygen vacancies were refilled. The direct interaction of N_2O with deposited carbon, leading to the formation of CO_2 and N_2 , could be

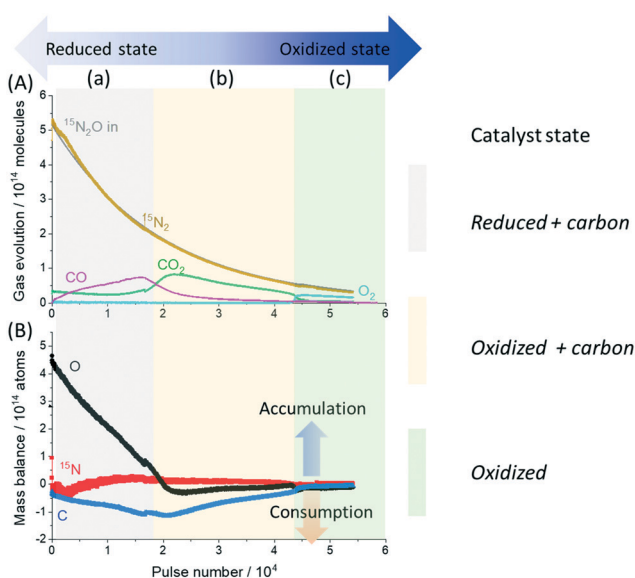


Fig. 3 A) Reactant and product evolution and B) ^{15}N , O, and C balance *versus* pulse number during the $^{15}\text{N}_2\text{O}$ multi-pulse experiment over C_3H_6 reduced Rh/CLZ at 450 °C; (a)–(c) represent the catalyst stage of the reduced catalyst with carbon deposits, oxidized catalyst with carbon deposits, and oxidized catalyst, respectively.

ruled out, since an identical N_2 response with a single characteristic peak was observed for both the C_3H_6 reduced and the H_2 reduced Rh/CLZ samples (Fig. S3, ESI†). The deposited carbon consumption decreased after pulse number 450 000. The ^{15}N species accumulation on the catalyst surface was insignificant. The ratio between N_2 and CO_2 was around 2 in the time interval between pulse numbers 10 000 and 450 000, which clearly demonstrated that for the formation of one CO_2 molecule two $^{15}\text{N}_2\text{O}$ molecules had to be reduced forming two $^{15}\text{N}_2$ molecules. Such a phenomenon suggested that the oxidation of one deposited carbon atom to CO_2 created two oxygen vacancies, which allowed for the reduction of two $^{15}\text{N}_2\text{O}$ molecules into two $^{15}\text{N}_2$ molecules. The formation of CO_2 started when the catalyst was largely oxidized, which suggested that CO_2 formed *via* a CO intermediate, which was subsequently oxidized into CO_2 by a ceria lattice oxygen. In previous studies,^{18,19} we have demonstrated that CO could reduce oxidized ceria up to almost one hypothetical ceria layer under identical reaction conditions.

Over H_2 reduced Rh/CLZ $^{15}\text{N}_2\text{O}$ reduction proceeded for approximately 3400 pulses (Fig. 1), while over C_3H_6 reduced Rh/CLZ this proceeded for approximately 45 000 pulses (Fig. 3); this remarkable difference indicated that the deposited carbon acted as a reductant buffer. N_2O was reduced over ceria oxygen vacancies, which led to the re-oxidation of these oxygen vacancies while N_2 was released at the same time. When most ceria oxygen vacancies were filled, ceria lattice oxygen became capable of oxidizing the carbon deposits into CO and CO_2 , thereby regenerating the ceria oxygen vacancies. The total amount of deposited carbon determined the additional ceria oxygen vacancies the Rh/CLZ system could provide, besides the ceria oxygen vacancies present after the reduction. The benefit of using hydrocarbons as reductants arose from the extended time interval in which 100% N_2O conversion was observed. In a previous publication we have demonstrated by means of an $^{18}\text{O}_2$ pulse experiment over C_3H_8 reduced Rh/CLZ at 450 °C that only lattice oxygen was responsible for the oxidation of deposited carbon, since only C^{16}O and C^{16}O_2 oxidation products containing exclusively ^{16}O from the CLZ lattice were observed.¹⁸

3.2.2. N_2O bond cleavage on a reduced catalyst. Fig. 4A shows the gas evolution during $^{15}\text{N}_2\text{O}$ and ^{14}NO co-pulses over a H_2 pre-reduced Rh/CLZ. The observed $^{15}\text{N}_2$ and $^{14}\text{N}_2$ products arose from the reduction of $^{15}\text{N}_2\text{O}$ and ^{14}NO , respectively. There was no evidence of any $^{14}\text{N}^{15}\text{N}$ and ^{15}NO formation. These experiments confirmed that $^{15}\text{N}_2\text{O}$ reduction proceeds *via* the dissociation of a ^{15}N –O bond of $^{15}\text{N}_2\text{O}$, of which O refilled a ceria oxygen vacancy and a desorbed $^{15}\text{N}_{2\text{g}}$ molecule was formed. Apparently, $^{15}\text{N}=\text{N}^{15}$ bond cleavage was absent, since $^{14}\text{N}^{15}\text{N}$ products were not observed. The transient kinetic data of $^{15}\text{N}_2$ and $^{14}\text{N}_2$ showed that $^{15}\text{N}_2$ formation was faster than $^{14}\text{N}_2$ formation, as $^{15}\text{N}_2$ was observed prior to $^{14}\text{N}_2$ (Fig. 4B). The formation of $^{14}\text{N}_2$ required the cleavage of the ^{14}NO bond and the subsequent association of two ^{14}N species, which was expected to proceed more slowly than $^{15}\text{N}_2$ formation *via* the direct cleavage of the ^{15}NO bond of $^{15}\text{N}_2\text{O}$.



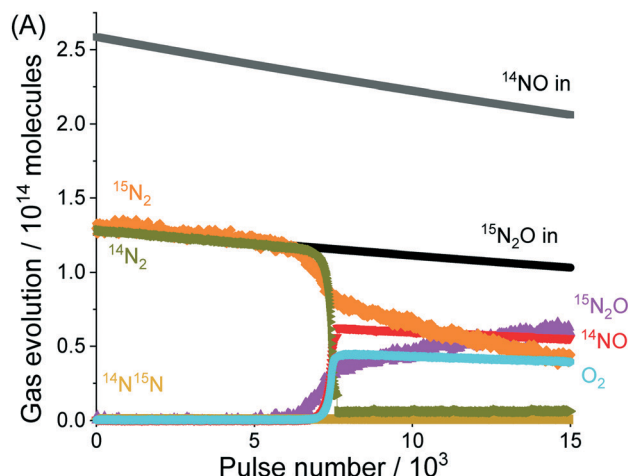


Fig. 4 A) Reactant and product evolution during $^{15}\text{N}_2\text{O}$ and ^{14}NO co-pulses over H_2 reduced Rh/CLZ at $450\text{ }^\circ\text{C}$ and B) the response of $^{15}\text{N}_2$ and $^{14}\text{N}_2$ averaged by the first 5000 pulses.

3.2.3. Effect of other oxidants on oxygen vacancy competition and deposited carbon consumption. In the Di-Air system, oxygen vacancies and buffer reductants (carbon deposits) were effectively re-created by periodical high frequency fuel injections. These vacancies were re-oxidized by the abstraction of oxygen atoms from oxidants present in the exhaust stream (H_2O , CO_2 , NO, N_2O , and O_2). The reactivity of these oxidants towards the ceria oxygen vacancies could depend on the reactivity of the O atoms in these oxidants. The reactivity of the O atoms in NO, CO_2 , and O_2 was investigated by pulsing each oxidant over C_3H_6 reduced Rh/CLZ.

As shown in Fig. 5A, all pulsed ^{15}NO converted to $^{15}\text{N}_2$ until the catalyst became oxidized. ^{15}NO is a powerful oxidant and is capable of filling all ceria oxygen vacancies (those on reduced CLZ and those created by the oxidation of carbon deposits by the CLZ lattice oxygen). The results presented in Fig. 4A suggested that the $^{15}\text{N}_2\text{O}$ reduction activity was not affected by the presence of ^{14}NO when the catalyst was in a reduced state. However, the $^{15}\text{N}_2\text{O}$ reduction activity was dramatically inhibited by NO when the catalyst switched to an oxidized state.

CO_2 fully converted into CO when the catalyst was in a significantly reduced state (Fig. 5B). However, when the catalyst was almost completely (re-)oxidized, the CO_2 reactivity suddenly dropped down while most of the deposited carbon was still on the Rh/CLZ surface (Fig. 5B). CO_2 hardly consumed any deposited carbon. A quasi-equilibrium between CO, CO_2 , Ce^{3+} , and Ce^{4+} appeared to limit the achievable oxidation degree of reduced ceria.¹⁹ Therefore, it can be concluded that CO_2 was a mild oxidant as compared to NO and N_2O , as it could hardly oxidize the deposited carbon. In the field of the dry CO_2 reforming of methane (DRM) reaction, the oxygen vacancies of a ceria support provided the catalytic sites for the CO_2 reduction to CO. The oxygen transport from the ceria lattice to the metal (Rh) largely reduced the carbon deposition during the DRM reaction.^{29,30} Fig. 5C shows the results obtained in an O_2 pulse experiment over C_3H_6 pre-reduced Rh/CLZ. O_2 was fully converted while CO and CO_2 formed

which originated from the oxidation of deposited carbon (Fig. 5C). O_2 broke through when the catalyst became oxidized. Therefore, O_2 was a strong oxidant, which can compete with NO and N_2O for oxygen vacancies. However, NO was a more reactive and competitive reactant towards the oxygen vacancies as compared to O_2 as evidenced in previously published experiments in which 500–2000 ppm NO and 5% O_2

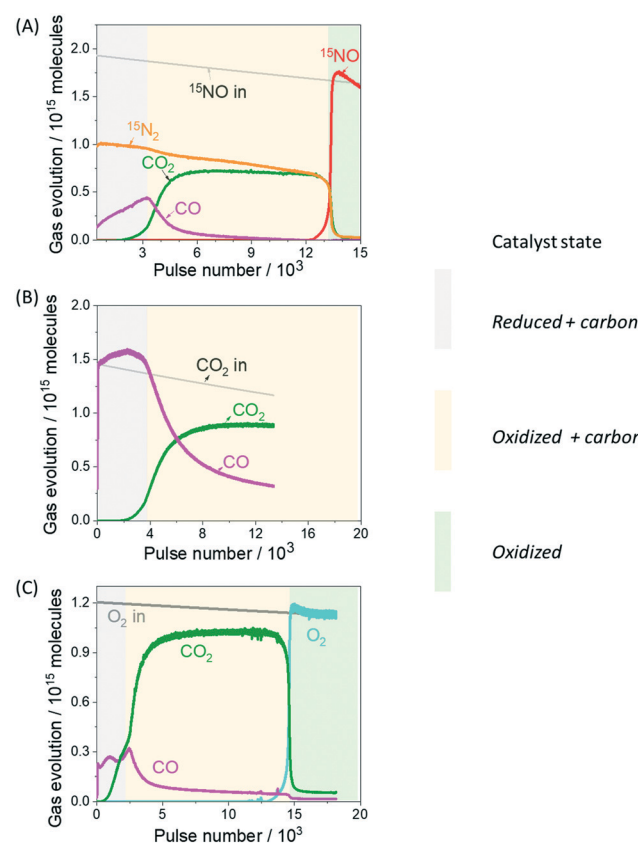


Fig. 5 Gas evolution during ^{15}NO (A), CO_2 (B), and O_2 (C) pulses over C_3H_6 pre-reduced Rh/CLZ at $450\text{ }^\circ\text{C}$.



were co-fed over C_3H_6 reduced Rh/CLZ at 450 °C.²¹ The current study presented in Fig. 4A suggested that N_2O was comparably reactive towards ceria oxygen vacancies as NO did, and therefore, N_2O was a more reactive and competitive reactant towards the oxygen vacancies as compared to O_2 .

In our previous publication, H_2 pulses over an oxidized ceria (CLZ) led to the formation of H_2O , yielding less than one monolayer of reduced ceria. This indicated the presence of a quasi-equilibrium established between H_2 , H_2O , Ce^{3+} , and Ce^{4+} , which limited the deeper reduction of ceria by H_2 or complete re-oxidation of reduced ceria by H_2O .¹⁹ Therefore, H_2O was a weaker oxidant towards oxygen vacancies. As a consequence, the presence of H_2O would not affect the NO and N_2O reduction over a reduced ceria. Ceria-based catalysts are among others the best candidates for the water gas shift reaction.^{31,32} Oxygen vacancies on the ceria surface played an essential role in the water dissociation, yielding H_2 while the oxygen atoms filled the ceria oxygen vacancies during the WGS reaction. The reaction of CO with ceria lattice oxygen led to the formation of CO_2 thereby recreating a ceria oxygen vacancy. The WGS reaction was an equilibrium-limited reaction. The water dissociation would produce H_2 and oxidize the reduced ceria while the formed CO_2 from CO would create the ceria oxygen vacancy. Therefore, the O reactivity of CO_2 and H_2O was expected to be relatively small and CO_2 and H_2O would not inhibit NO and N_2O reduction into N_2 to a large extent.

3.3. Catalytic fixed-bed reactor evaluation with regard to a potential industrial application

To confirm the results obtained in the TAP experiments, similar experiments were performed over Rh/CLZ in a flow reactor at atmospheric pressure and industrial exhaust concentrations. Similar to the TAP experiment, the flow of 1.25% C_3H_6 /He in a fixed-bed reactor at 450 °C for 2 h led to the formation of H_2O , CO_2 , CO, H_2 and carbon on the catalyst surface. The quantification of the oxygen and carbon balance was performed, according to eqn (1) and (2), respectively, and showed a reduction of around 3 CLZ layers and deposition of 8.2×10^{17} carbon atoms per mg_{cat} . N_2O reduction over the C_3H_6 pre-reduced Rh/CLZ was investigated under a gas mixture of 2000 ppm N_2O /He, (2000 ppm N_2O + 5% O_2)/He, and (2000 N_2O ppm + 2000 ppm NO)/He. Both MS and FTIR were used to detect the gas evolution. $m/z = 28$ can be attributed to either CO or N_2 , and $m/z = 44$ to either CO_2 or N_2O . Gas species which contributed to the vibration peaks in the FT-IR spectrum can be seen in Table 1.

Fig. 6 shows the results of the exposure of a C_3H_6 reduced Rh/CLZ catalyst to 2000 ppm N_2O at 450 °C with a GHSV of 67 000 L $L^{-1} h^{-1}$. In Fig. 6A, $m/z = 28$ was observed, which could be attributed to the formation of N_2 and CO. The formation of CO was confirmed by FT-IR (Fig. 6B). The CO yield increased up to a maximum of 2500 ppm, after which it declined to zero (Fig. 6B and C). After CO had vanished ($t = 1000$ s), $m/z = 28$ was still observed in the MS (Fig. 6A). There-

Table 1 FT-IR wavenumbers of different gas species

Wavenumber/cm ⁻¹	Gas species
2350	CO_2
2235 and 2208	N_2O
2174 and 2116	CO
1908 and 1850	NO
1601 and 1628	NO_2

fore, in addition to CO, N_2 also contributed to $m/z = 28$. $m/z = 44$ was observed between 400 s and 1500 s, which could be attributed to the formation of CO_2 and the slip of N_2O . The formation of the latter could be excluded, during this time interval, FT-IR results indicated the absence of peaks at 2235 and 2208 cm⁻¹ and the presence of a peak at 2350 cm⁻¹, which confirmed the formation of CO_2 and excluded the presence (slip) of N_2O in the reactor effluent. The formation of CO and CO_2 indicated the oxidation of deposited carbon by the reduction of N_2O . No NO or NO_2 formation was observed during the whole experiment. N_2O was completely converted into N_2 as evidenced by FTIR where no N_2O and/or NO_2 peaks were observed within the detection limit of 1 ppm. The observation of N_2 in the MS indicated an extremely selective reduction of N_2O into N_2 . O_2 arising from N_2O started to break through roughly from 1400 s onward, while the CO_2 yield started to decrease. The breakthrough of O_2 implied that the catalyst was largely oxidized and coincided with the disappearance of CO and CO_2 from the FTIR spectrum, indicating that all deposited carbon was oxidized. These observations indicated that the N_2O reduction over C_3H_6 pre-reduced Rh/CLZ consisted of the refilling of the oxygen vacancies and the oxidation of the carbon deposits. Overall, the results presented in Fig. 6 clearly demonstrate that the HC pre-reduced Rh/CLZ catalyst exhibited excellent N_2O reduction performance, which was in line with the conclusion from the TAP study (Fig. 3).

In order to explore the performance of Rh/CLZ in real industrial applications, a good catalytic activity for only N_2O is not sufficient. The N_2O reduction activity has to be studied in the presence of potential inhibitors in the exhaust stream under atmospheric pressure. NO and O_2 are the most challenging inhibitors as they both can compete with N_2O for the oxygen vacancies. Fig. 7 and 8 summarize the results obtained in the presence of O_2 and NO.

The influence of O_2 addition to the N_2O (2000 ppm) gas feed on N_2O reduction is shown in Fig. 7. O_2 ($m/z = 32$) started to break through after approximately 20 s, while N_2O was not observed (detection limit of 1 ppm) until 160 s. From that point on around 25 ppm N_2O was detected by FT-IR. The N_2O breakthrough time was 8× later than that of O_2 (50 000 ppm), which indicated that a small concentration of N_2O (2000 ppm) was able to compete with an excess of O_2 . NO and NO_2 were not detected anytime in the reactor effluent. This clearly suggested that N_2O could be selectively reduced into N_2 in the presence of O_2 . The observation of 25 ppm of N_2O after O_2 breakthrough (Fig. 7C), i.e., 98.8% N_2O



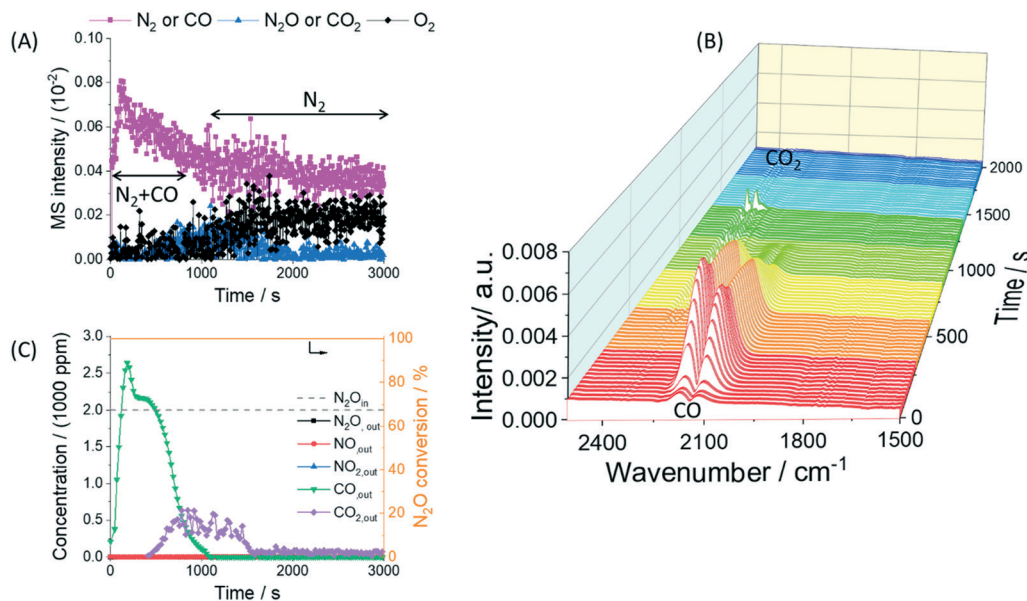


Fig. 6 Gas evolution during the exposure of C_3H_6 reduced Rh/CLZ to 2000 ppm N_2O in He at $450\text{ }^\circ\text{C}$. A) MS responses, B) FT-IR spectral responses, and C) quantification of (B).

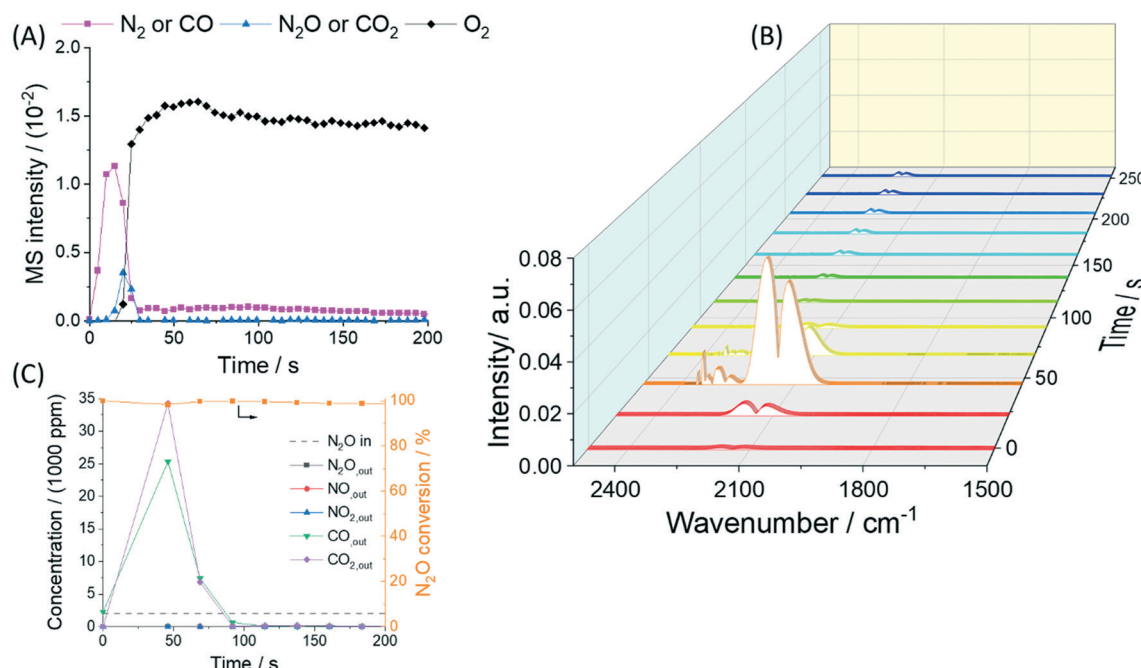


Fig. 7 Gas evolution during the exposure of C_3H_6 reduced Rh/CLZ to 2000 ppm N_2O + 5 vol% O_2 in He at $450\text{ }^\circ\text{C}$. A) MS responses, B) FT-IR spectral responses, and C) quantification of (B).

conversion, suggested that the presence of O_2 inhibited the catalytic reduction of N_2O to a very small extent when the catalyst became oxidized. These results indicated that the reduction of N_2O into N_2 over reduced Rh/CLZ was not affected by the addition of O_2 . N_2O was much more competitive towards the oxygen vacancies as compared to O_2 .

Fig. 8 evaluates the effect of adding NO to the N_2O gas feed. N_2O and NO roughly broke through at the same time while CO formation decreased, which indicated that N_2O and

NO compete equally for the active sites. The presence of NO did not affect the reduction of N_2O into N_2 , while the deposited carbon was oxidized. Only 100 ppm of NO_2 was observed when NO appeared in the reactor effluent as noticed in the FT-IR spectrum (Fig. 8C). This NO_2 likely formed due to the reaction of NO with surface oxygen species in the N_2O reduction through steps (8)–(10):



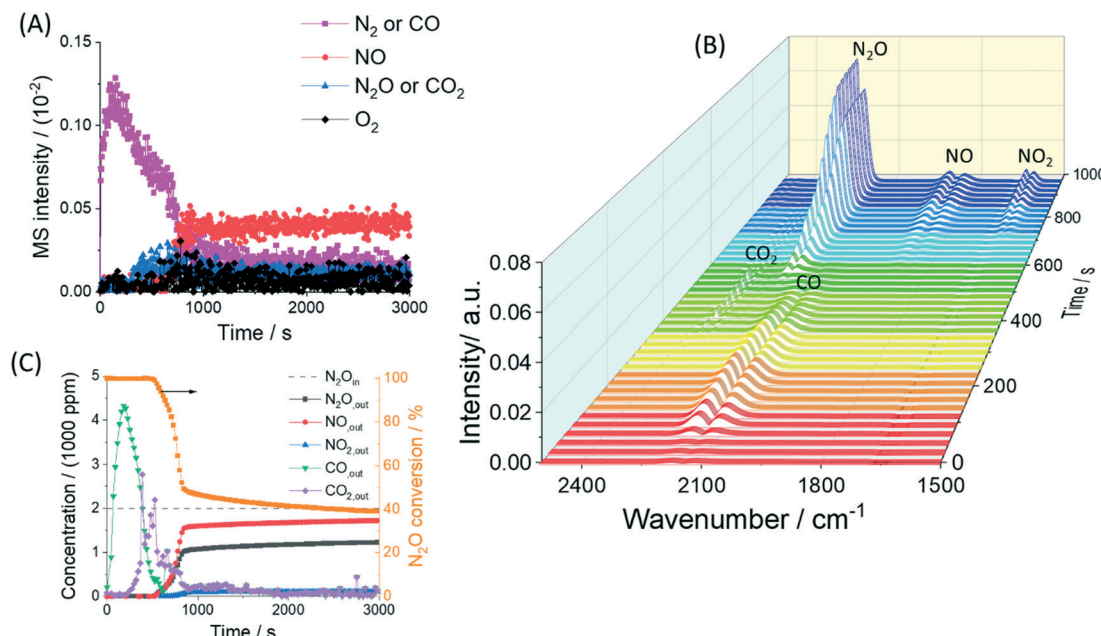


Fig. 8 Gas evolution during the exposure of C_3H_6 reduced Rh/CLZ to 2000 ppm N_2O + 2000 ppm NO in He at 450 °C. A) MS responses, B) FT-IR spectral responses, and C) quantification of (B).



When there was no deposited carbon on the surface, NO affected the N_2O reduction dramatically, while this was less significant when co-feeding only O_2 . The detection of NO_2 over the oxidized sample implied that surface nitrite and nitrate species formed on the catalyst surface catalyzed by the rhodium surface sites. The formation of NO_2 could proceed *via* the reaction of NO with surface O species, which originated either from N_2O reduction or catalyst surface lattice oxygen. These surface nitrite and nitrate species would affect the surface oxygen species mobility, and the O_2 association and desorption from the Rh sites.³³ Another NO_2 formation pathway could proceed *via* the disproportionation of NO into N_2 and NO_2 . The discrimination between and/or the extent of contribution of the two pathways was beyond the scope of this study.

Fig. 9 summarizes the observed N_2O conversion for the different gas feeds over O_2 pre-oxidized and C_3H_6 pre-reduced Rh/CLZ. For N_2O , the catalyst displayed 100% N_2O conversion over both O_2 pre-oxidized and C_3H_6 pre-reduced samples. For $\text{N}_2\text{O} + \text{O}_2$ (excess), the N_2O conversion dropped from 100% to 98.8% when the catalyst switched from a reduced to an oxidized state. For $\text{N}_2\text{O} + \text{NO}$, the conversion of N_2O dropped from 100% to 37% when the catalyst switched from a reduced into an oxidized state. The inhibition of the N_2O reduction by NO was a common issue in the N_2O abatement, since the majority of explored catalysts had a very low tolerance towards NO. In summary, the above experiment clearly demonstrated that a C_3H_6 pre-reduced Rh/CLZ catalyst

exhibited a unique and extraordinary N_2O reduction performance, when the Rh/CLZ was in a reduced state. Again, carbon deposits extended the time frame during which the Rh/CLZ catalyst remained reduced.

Besides our previous publication,¹⁷ the experiment of (5% CO_2 + 2000 ppm NO)/He over C_3H_6 pre-reduced Rh/CLZ in a fixed bed flow reactor indicated that NO by far was a more powerful reductant in the competition for the oxygen vacancies as compared to CO_2 . Around 90% of the deposited carbon was consumed by NO *via* the lattice oxygen of the ceria. NO was selectively reduced into N_2 regardless of the CO_2 presence.¹⁷ The presence of CO_2 did not affect the NO reactivity and selectivity over the reduced CLZ and Rh/CLZ catalysts. The presence of CO_2 would, therefore, not affect both the N_2O and NO reduction into N_2 over reduced Rh/CLZ.

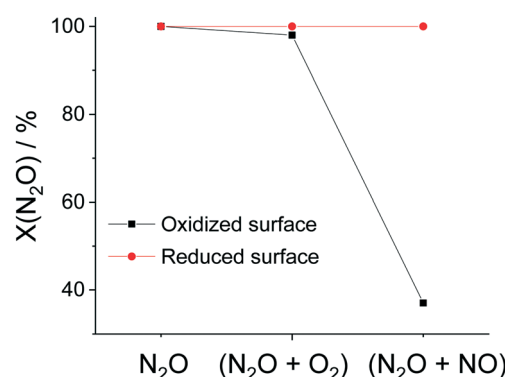


Fig. 9 N_2O conversion over O_2 pre-oxidized and C_3H_6 pre-reduced Rh/CLZ in 2000 ppm N_2O in He, 2000 ppm N_2O + 5% O_2 in He, and 2000 ppm N_2O + 2000 ppm NO in He. Conditions: atmospheric pressure, 450 °C, and GHSV = 67 000 L L⁻¹ h⁻¹.

4. Conclusion

This work shows that a C₃H₆ pre-reduced Rh/CLZ catalyst exhibits a unique and extraordinary performance in the reduction of N₂O in the presence of other oxidants, *e.g.*, most importantly O₂ and NO. The reductive pretreatment with C₃H₆ created oxygen vacancies and carbon deposits on the Rh/CLZ surface. These oxygen vacancies were the catalytic sites for an extremely selective reduction of N₂O into N₂, in which the oxygen vacancies were replenished. The deposited carbon acted as a buffer reductant and was responsible for the generation of new oxygen vacancies. This new N₂O reduction system could be cycled by short pulses of hydrocarbons upstream of the catalyst bed, which allowed regeneration of the oxygen vacancies and deposited carbon. Our work clearly indicated that the Di-Air DeNO_x system could be applied in simultaneous NO_x and N₂O reduction under oxygen rich conditions, using a single Rh/CLZ catalyst bed, under industrial relevant conditions.

Conflicts of interest

There are no conflicts to be declared.

References

- 1 E. A. Davidson and D. Kanter, *Environ. Res. Lett.*, 2014, **9**, 105012.
- 2 F. Kapteijn, J. Rodriguez-Mirasol and J. A. Moulijn, *Appl. Catal., B*, 1996, **9**, 25–64.
- 3 P. Esteves, Y. Wu, C. Dujardin, M. Dongare and P. Granger, *Catal. Today*, 2011, **176**, 453–457.
- 4 A. Adamski, W. Zająć, F. Zasada and Z. Sojka, *Catal. Today*, 2012, **191**, 129–133.
- 5 H. Zhou, P. Hu, Z. Huang, F. Qin, W. Shen and H. Xu, *Ind. Eng. Chem. Res.*, 2013, **52**, 4504–4509.
- 6 F. Perez-Alonso, I. Melián-Cabrera, M. L. Granados, F. Kapteijn and J. G. Fierro, *J. Catal.*, 2006, **239**, 340–346.
- 7 S. Gudyka, G. Grzybek, J. Gryboś, P. Indyka, B. Leszczyński, A. Kotarba and Z. Sojka, *Appl. Catal., B*, 2017, **201**, 339–347.
- 8 G. Delahay, M. Mauvezin, B. Coq and S. Kieger, *J. Catal.*, 2001, **202**, 156–162.
- 9 J. Pérez-Ramírez, J. García-Cortés, F. Kapteijn, M. Illán-Gómez, A. Ribera, C. S. M. de Lecea and J. A. Moulijn, *Appl. Catal., B*, 2000, **25**, 191–203.
- 10 M. K. Kim, P. S. Kim, B. K. Cho, I.-S. Nam and S. H. Oh, *Catal. Today*, 2012, **184**, 95–106.
- 11 M. Inger, J. Rajewski, M. Ruszak and M. Wilk, *Chem. Pap.*, 2019, **1**–8.
- 12 M. Kögel, R. Mönnig, W. Schwieger, A. Tissler and T. Turek, *J. Catal.*, 1999, **182**, 470–478.
- 13 F. Schuricht and W. Reschetilowski, *Microporous Mesoporous Mater.*, 2012, **164**, 135–144.
- 14 M. C. Campa, D. Pietrogiacomi, C. Scarfiello, L. R. Carbone and M. Occhiuzzi, *Appl. Catal., B*, 2019, **240**, 367–372.
- 15 Y. Bisaiji, K. Yoshida, M. Inoue, K. Umemoto and T. Fukuma, *SAE Int. J. Fuels Lubr.*, 2012, **5**, 380–388.
- 16 Y. Wang, J. P. de Boer, F. Kapteijn and M. Makkee, *ChemCatChem*, 2016, **8**, 102–105.
- 17 Y. Wang and M. Makkee, *Appl. Catal., B*, 2018, **221**, 196–205.
- 18 Y. Wang, F. Kapteijn and M. Makkee, *Appl. Catal., B*, 2018, **231**, 200–212.
- 19 Y. Wang and M. Makkee, *Appl. Catal., B*, 2018, **223**, 125–133.
- 20 Y. Wang and M. Makkee, *Appl. Catal., B*, 2019, **259**, 117895.
- 21 Y. Wang, R. Oord, D. Van Den Berg, B. M. Weckhuysen and M. Makkee, *ChemCatChem*, 2017, **9**, 2935–2938.
- 22 S. Parres-Escalpez, I. Such-Basañez, M. Illán-Gómez, C. S.-M. de Lecea and A. Bueno-López, *J. Catal.*, 2010, **276**, 390–401.
- 23 H. Abderrahim and D. Duprez, in *Studies in Surface Science and Catalysis*, ed. A. Crucq and A. Frennet, Elsevier, 1987, vol. 30, pp. 359–368.
- 24 C. Desorme and D. Duprez, *Appl. Catal., A*, 2000, **202**, 231–241.
- 25 E. V. Kondratenko, V. A. Kondratenko, M. Santiago and J. Pérez-Ramírez, *J. Catal.*, 2008, **256**, 248–258.
- 26 Y. Wang, M. R. Kunz, S. Siebers, H. Rollins, J. Gleaves, G. Yablonsky and R. Fushimi, *Catalysts*, 2019, **9**, 104.
- 27 Y. Wang, R. Kunz, P. D. D. Constales, G. Yablonsky and R. R. Fushimi, *J. Phys. Chem. A*, 2019, **123**, 8717–8725.
- 28 Y. Wang, M. R. Kunz, Z. Fang, G. Yablonsky and R. R. Fushimi, *Ind. Eng. Chem. Res.*, 2019, **58**, 10238–10248.
- 29 I. V. Yentekakis, G. Goula, M. Hatzisymeon, I. Betsi-Arygropoulou, G. Botzolaki, K. Kousi, D. I. Kondarides, M. J. Taylor, C. M. A. Parlett, A. Osatiashvili, G. Kyriakou, J. P. Holgado and R. M. Lambert, *Appl. Catal., B*, 2019, **243**, 490–501.
- 30 G. Goula, G. Botzolaki, A. Osatiashvili, C. Parlett, G. Kyriakou, R. M. Lambert and I. V. Yentekakis, *Catalysts*, 2019, **9**, 541.
- 31 D. Pal, R. Chand, S. Upadhyay and P. Mishra, *Renewable Sustainable Energy Rev.*, 2018, **93**, 549–565.
- 32 J. Vecchietti, A. Bonivardi, W. Xu, D. Stacchiola, J. J. Delgado, M. Calatayud and S. E. Collins, *ACS Catal.*, 2014, **4**, 2088–2096.
- 33 M. Zabilskiy, P. Djinović, E. Tchernychova and A. Pintar, *Appl. Catal., B*, 2016, **197**, 146–158.

